Graphene Membranes with Tunable Nanometer-Scale Pores

Rohit N. Karnik (PI)
Department of Mechanical Engineering, Massachusetts Institute of Technology
77 Massachusetts Avenue, MIT Room 3-461A, Cambridge MA 02139
Email: karnik@mit.edu; Web: http://meche.mit.edu/people/faculty/karnik@mit.edu

Award number: DE-SC0008059

Collaborators: Dr. Juan-Carlos Idrobo, Oak Ridge National Laboratory, Oak Ridge, TN 37831
Dr. Nicolas Hadjiconstantinou, Massachusetts Institute of Technology, Cambridge, MA 02139
Dr. Jing Kong, Massachusetts Institute of Technology, Cambridge, MA 02139
Dr. Tahar Laoui, King Fahd University of Petroleum and Minerals, Saudi Arabia

Executive summary: Graphene, a one-atom thick material comprising hexagonally bonded carbon atoms, is one of the strongest materials known and is impermeable to even helium gas. The potential for creation of tunable nanometer-scale pores in graphene, combined with mechanical strength, chemical resistance, and atomic thickness, make it a promising material for improving selectivity, permeability, and energy efficiency in a diverse range of membrane separations. However, fundamental understanding of creation of porous graphene, its mass transport properties, and the relationship between porosity and membrane performance is lacking. This project studied methods to create pores in graphene by ion irradiation and etching, and investigated the effect of the porosity of graphene on mass transport properties at the membrane level as well as across individual pores. Detailed characterization of pore size distributions in graphene using high-resolution scanning transmission electron microscopy was performed to elucidate the relationship between different pore creation processes and the resulting porosity. New methods to create tunable nanometer-scale pores in graphene at high density over large areas were developed. Graphene membranes were fabricated comprising single-layer porous graphene on appropriate support membranes. Mass transport of ions, molecules, water, and gases across the membranes was investigated, and predictive models were developed to relate the graphene porosity and support membrane structure to the mass transport properties of the membranes. The effect of graphene porosity on permeance of the membranes to water, salts, and small molecules was experimentally quantified. Single-pore measurements were performed and a model was developed to understand ion transport across graphene pores, which led to the experimental observation of heterogeneity in transport behaviors and spontaneous fluctuations of ion transport. Functional single-layer nanoporous graphene membranes comprising a high density of pores over macro-scale areas with molecular selectivity were demonstrated for the first time. This project led to three patent applications and 9 journal articles. The fundamental developments in understanding nanoporous graphene membranes have laid the foundations to develop energy-efficient nanoporous graphene membranes for various applications in water desalination, oil and natural gas separations, biotechnology, and chemical processing.

Overall research goals: Graphene, a one-atom thick membrane of hexagonally bonded carbon atoms, is one of the strongest materials known and is impervious to the diffusion of even helium gas. The potential for creation of tunable nanometer-scale pores in graphene, combined with its other properties, make it a promising material for improving selectivity, permeability, and energy efficiency in a diverse range of membrane separation and sensing applications. The research objectives of this project were to systematically study the effect of pore creation methods (ion irradiation, nitrogen doping, and chemical oxidation) to create tunable, nanometer-scale pores in

graphene membranes. We aimed to use high-resolution imaging to study the pore structures and to elucidate the resulting transport characteristics of the membranes at the single pore and ensemble levels. The specific questions that this project sought to answer are as follows:

1. What are the pore structures and densities in graphene membranes created by ion bombardment, nitrogen doping, and chemical oxidation?
2. How does ionic and molecular transport through pores in graphene membranes depend on constituent pore structures, and ionic/molecular charge and size?
3. How can pores in graphene membranes be tailored to achieve desired transport characteristics for specific applications?
4. What is the inherent heterogeneity in ionic transport through single pores, and how does it determine transport through a membrane consisting of a multitude of pores?

This work sought to advance our understanding of mass transport across nanopores in graphene and to lay the foundations for the development of nanoporous graphene membranes.

Accomplishments:

A central hypothesis of this work is that the transport of different ions and molecules across a layer of graphene can be tuned by creating appropriately sized pores in the graphene. We used graphene composite membranes by transferring graphene grown on copper foil to a polycarbonate track-etched membrane support as a platform for the study of transport through pores in graphene, while transfer to a TEM substrate was used for imaging to characterize the pores. A platform comprising graphene suspended over a pore in a silicon nitride (SiN_x) membrane was used to probe transport across isolated pores in graphene. Studies were also performed in parallel to understand the critical role of defects in determining the transport across porous graphene. Accomplishments arising from work funded fully or in part by this project with respect to the original project goals are summarized as follows:

1. What are the pore structures and densities in graphene membranes created by ion bombardment, nitrogen doping, and chemical oxidation? *Results*: Extensive characterization of pore size distributions using scanning transmission electron microscopy (STEM) was undertaken. The studies resulted in the most detailed quantitative measurement of the effect of ion irradiation, chemical/plasma oxidation, and their combinations on the resulting porosity available in the literature, providing insights into how pore size distributions evolve under these treatments. Rather than nitrogen doping, a similar in situ method for pore creation was explored by simply tuning the temperatures during graphene synthesis.
2. How does ionic and molecular transport through pores in graphene membranes depend on constituent pore structures, and ionic/molecular charge and size? *Results*: Extensive measurements of diffusion of salts and small molecules, and forward osmosis of water were performed on membranes with different pore size distributions characterized by STEM. Transport of different gas molecules was also measured. The fundamental transport properties of graphene were extracted from the measurements. These properties were related to the membrane porosity using continuum models, with good agreement. These results are the only ones to report on quantitative measurements of both the pore size distributions and the mass transport properties of graphene for nanometer to sub-nanometer pores.
3. How can pores in graphene membranes be tailored to achieve desired transport characteristics for specific applications? *Results*: The ability to tailor pores and mass transport in the sub-nanometer to ~4 nm range was demonstrated. It was shown that control of pore creation parameters can be used to control the selectivity and mass transport across graphene. Rejection of small molecules and multivalent salts was demonstrated as a potential example of

nanofiltration. Ultrahigh permeance separation of gas molecules was also demonstrated through tuning of the pore size. Chemical separation by dialysis (diffusion) was also shown.

4. What is the inherent heterogeneity in ionic transport through single pores, and how does it determine transport through a membrane consisting of a multitude of pores? *Results*: Ion transport was investigated across isolated pores in graphene. It was found that different pores exhibit quite distinct transport behaviors and sometimes exhibited spontaneous fluctuations in ionic current. The observations were explained by a model that incorporated electrostatic and ion hydration interactions. Multi-scale models were built to relate the pore size distributions and graphene support structure to mass transport across the membrane. These models provide a fair degree of predictive ability and also reveal how defects in graphene can impact mass transport across the membranes.

Accomplishments are described in more detail below.

Understanding the creation of sub-nanometer pores in graphene:

We developed a generalized approach to pore creation that comprises the steps of (1) nucleation of defects followed by (2) oxidative etching to form pores. In the first set of experiments, we used ion bombardment (8 kV, 52° incidence, at a dose of 10^{13} ions/cm^2) to induce defects in the graphene lattice, and experimented with different oxidizers to identify that a mixture of potassium permanaganate and sulfuric acid (reported by Kosynkin et al *Nature*, 2009) to unzip carbon nanotubes) could create subnanometer pores in the ion-bombarded graphene (Figure 1a,b). Detailed STEM characterization showed that the pore density increased with etch time and approached the ion bombardment density, but the pore size increased only slightly with etch time and stabilized at ~0.4 nm (Figure 1c). Although STEM imaging did not reveal pore formation before etching, Raman characterization showed the emergence of defect peaks upon ion bombardment, and the gradual

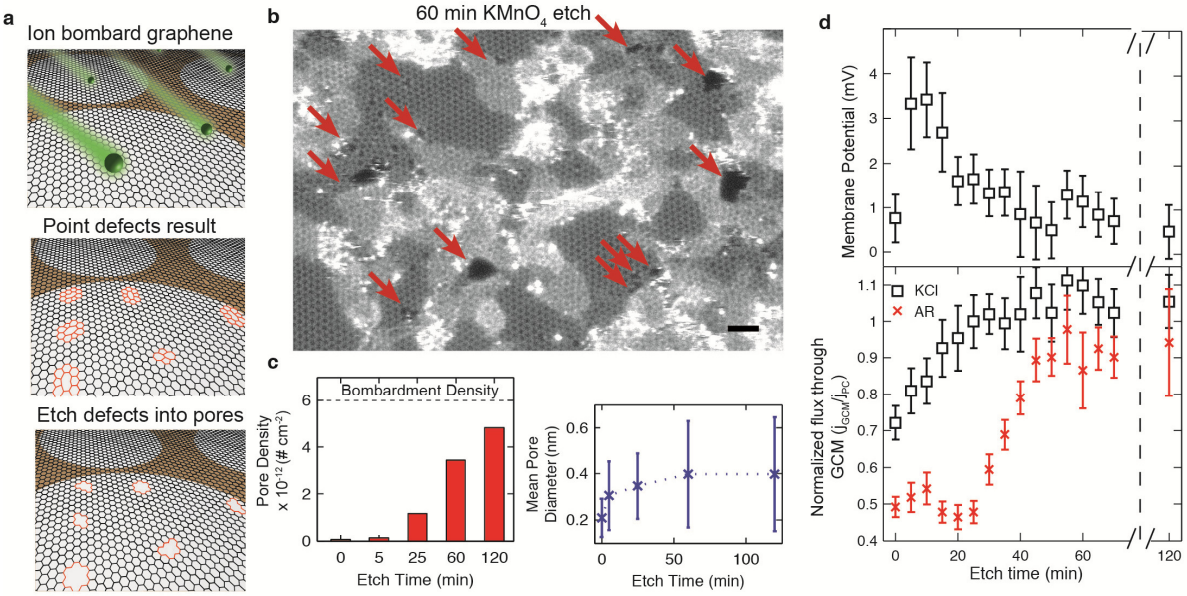

Figure 1. a) Gallium ion bombardment of graphene results in defects that open into permeable pores after potassium permanganate etching. b) STEM image of pores created in graphene. c) Pore density approaches bombardment density at the 120 min time, while the mean pore diameter stabilizes at 0.4 ± 0.24 nm. d) Increase in membrane potential indicates cation selective transport at the 5-10 min etch time, while higher flux of the KCl transport over Allura Red AC (~1 nm model organic molecule) indicates size-selective transport, reaching a maximum selectivity at the 25 min etch time.

disappearance of the graphene lattice peaks as etching progressed, which was consistent with pore formation observed in STEM. XPS studies showed that the etching process led to formation of C-O and C=O bonds, suggesting that the pores were decorated with hydroxyl, ketone, quinone, carbonyl, or similar groups. These observations taken together suggest a mechanism of pore creation wherein ion bombardment creates amorphous or damaged areas of graphene that begin etching with some delay upon exposure to the etchant, but then etch quickly and stabilize at the final pore size. We also demonstrated that these pores were able to impart selectivity to graphene (Figure 1d).

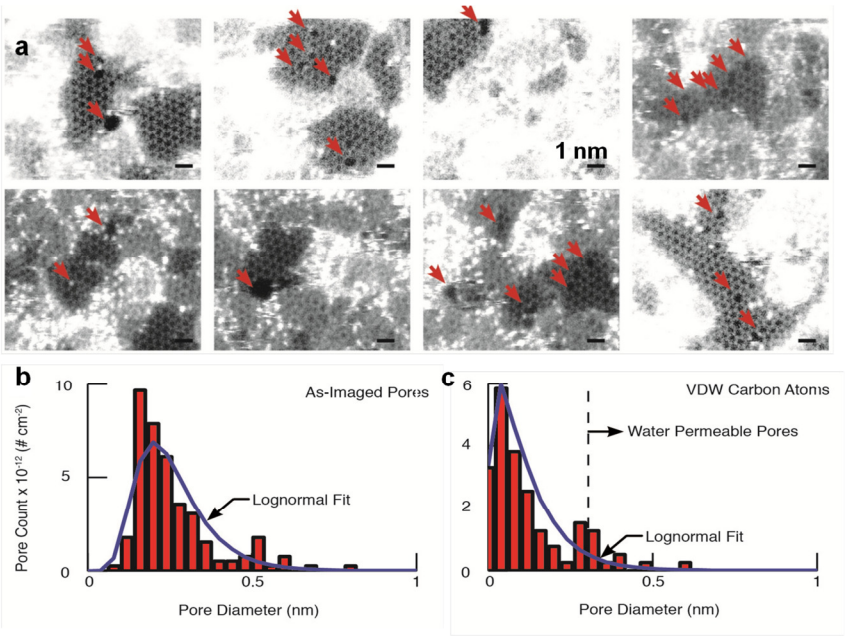

Figure 2. a) STEM images of pores in graphene formed by irradiation with gallium ions at 0° incidence, $7x10^{13}$ cm^{-2} dose, and 1 kV energy, followed by 60 min etch in acidic permanganate solution. Pore size distributions of as-imaged pores (b) and after adjusting for van der Waals size of carbon (c).

Following on this work, we varied the ion irradiation parameters. We changed the ion bombardment angle to perpendicular (0°) incidence, ion dose to $7x10^{13}$ cm^{-2}, and energy to 1 kV. These parameters are predicted to yield smaller defects (Lehtinen et al *Nanotechnology*, 2011), and presumably smaller pores that may exhibit selective transport of water. We found that the number density of pores was $3.9x10^{13}$ cm^{-2}, approximately half that of the incident ion dose. The pores were also smaller in size as compared to those formed with inclined incidence, with a mean as-measured pore size of 0.28 nm and effective size of 0.16 nm after accounting for van der Waals size of the atoms. Since water molecule size is 0.275 nm, in fact many pores were smaller than the size of water molecules (Figure 2).

According to simulations by Lehtinen et al (*Nanotechnology*, 2011), inclined bombardment of ions creates defects in the form of amorphous regions, with each incident ion having a high probability of forming a defect. With vertical irradiation, the probability of forming defects a little lower, and most defects are single or double vacancies as opposed to amorphous regions. The results suggest the validity of the simulations, and portray a mechanism of pore creation where only amorphous regions are removed by the mild permanganate etch. These results, published in Nano Letters in 2014 & 2015, contribute to understanding of the effects of ion irradiation and oxidation on the size and structure of pores created in graphene, which had previously been confined to theoretical predictions.

Study of mass transport across nanoporous graphene:

We performed measurements of transport of salts and solutes across nanoporous graphene driven by concentration gradients, and also developed methods to study water transport and solute rejection by forward osmosis.

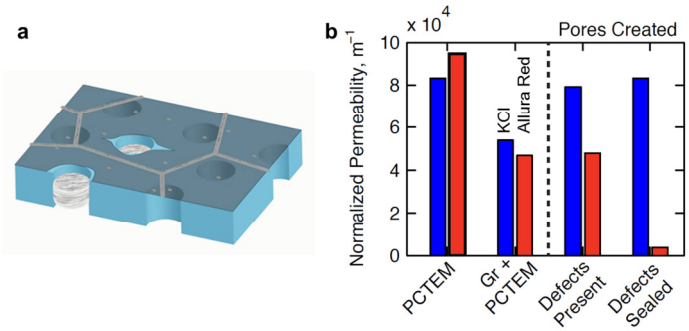

Figure 3. a) Schematic of leak-sealed membrane. b) Normalized diffusive permeability (inverse of effective thickness) of KCL (blue) and Allura Red (red) under different conditions. Left to right: Permeability of bare polycarbonate support (PCTEM) decreases when graphene is placed on the PCTEM (Gr + PCTEM), but there is transport through defects and no selectivity. Creating KCl-selective pores increases KCl transport while keeping Allura transport unchanged. Sealing leaks and then creating KCl-selective pores results in highly selective KCl transport.

Diffusive transport measurements of KCl and Allura Red (~1 nm sized model organic molecule) on centimeter-sized membranes with pores created using inclined ion bombardment illustrated the ability to control selectivity of the membrane based on chemical etch time (Figure 1d). We observed cation selectivity at short etch times as evidenced by an increase in the membrane potential, which was predicted theoretically (Zhao et al *J Chem Phys* 139, 114702, 2013) for nanoporous graphene but had not been experimentally observed. At longer etch times the graphene layer permitted transport of salt while blocking the larger organic molecule. This range of selectivity is useful for dialysis and nanofiltration applications.

We used a transport resistance network model to isolate the transport characteristics of the created subnanometer pores in graphene. This model essentially subtracted out the effect of parallel leakage pathways, allowing us to estimate the permeabilities and selectivity of only the created pores. The model suggested that the subnanometer pores had ~30-fold selectivity between KCl and Allura Red. The permeability extracted from experimental measurements agreed with theoretical estimates of the graphene permeability calculated using a continuum size-exclusion model based on the pore size distributions measured by STEM. This agreement further indicates that the created pores were responsible for the selective transport behavior.

To directly probe transport across graphene without large parallel leakage pathways as in the diffusion experiments in Figure 1d, we performed transport experiments on graphene membranes with leaks sealed using methods that we separately developed. This approach used a combination of

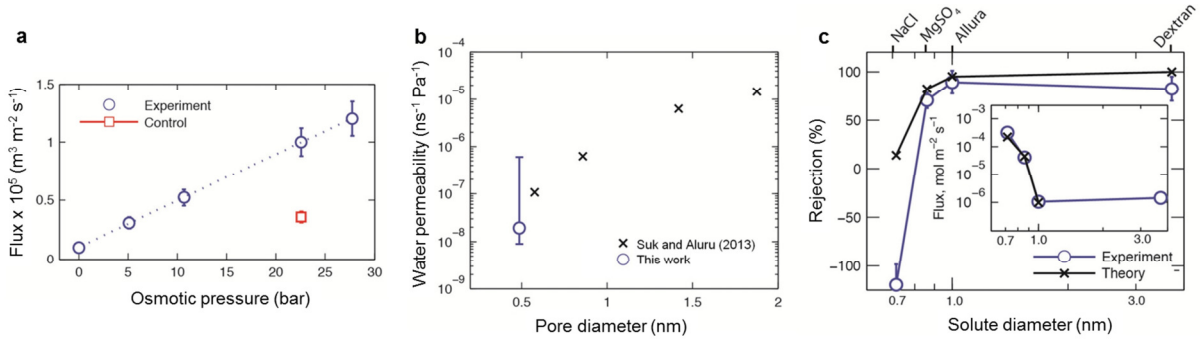

Figure 4. a) Measured flux of water across graphene under forward osmosis. Control is membrane with only the ion irradiation step omitted. b) Estimated permeance of graphene pores to water compared to simulations by Suk and Aluru (*RSC Adv* 2013). c) Rejection and flux of different solutes during forward osmosis.

atomic layer deposition and interfacial polymerization to first seal leakage pathways, resulting in a membrane where a monolayer of graphene separates the two sides (Figure 3a). We then created subnanometer pores in the graphene and obtained an actual KCl/Allura Red selectivity exceeding 40 for diffusive transport (Figure 3b), in agreement with the selectivity estimated from the previous study on leaky membranes.

Sealing of leakage pathways also allowed for forward osmosis experiments to quantify the permeability of monolayer nanoporous graphene for water. Using vertical irradiation of ions to create pores, we measured transport of water as well as rejection of different solutes under forward osmosis. We found that the water flux increased linearly with osmotic pressure (Figure 4a), and corresponded to a permeance of the graphene of 1.4 ± 0.2 L m^{-2} h^{-1} bar^{-1}, which is comparable to permeance of seawater reverse osmosis membranes. By estimating the number density of water-permeable pores in graphene, we were able to estimate the permeance of graphene nanopores (Figure 4b). The experimental measurements agreed with the trends predicted by molecular dynamics simulations (Suk and Aluru, *RSC Adv* 2013), suggesting their validity in predicting water transport across pores in graphene.

Finally, we measured the rejection of different solutes when water was drawn across graphene by forward osmosis. We found that the membranes effectively rejected Allura Red (~ 1 nm), dextran (~3 nm) with rejection ~90%, and also rejected $MgSO_4$ by ~70% (Figure 4c). However, we found that NaCl could easily diffuse across leaks in the membrane which resulted in a negative value for

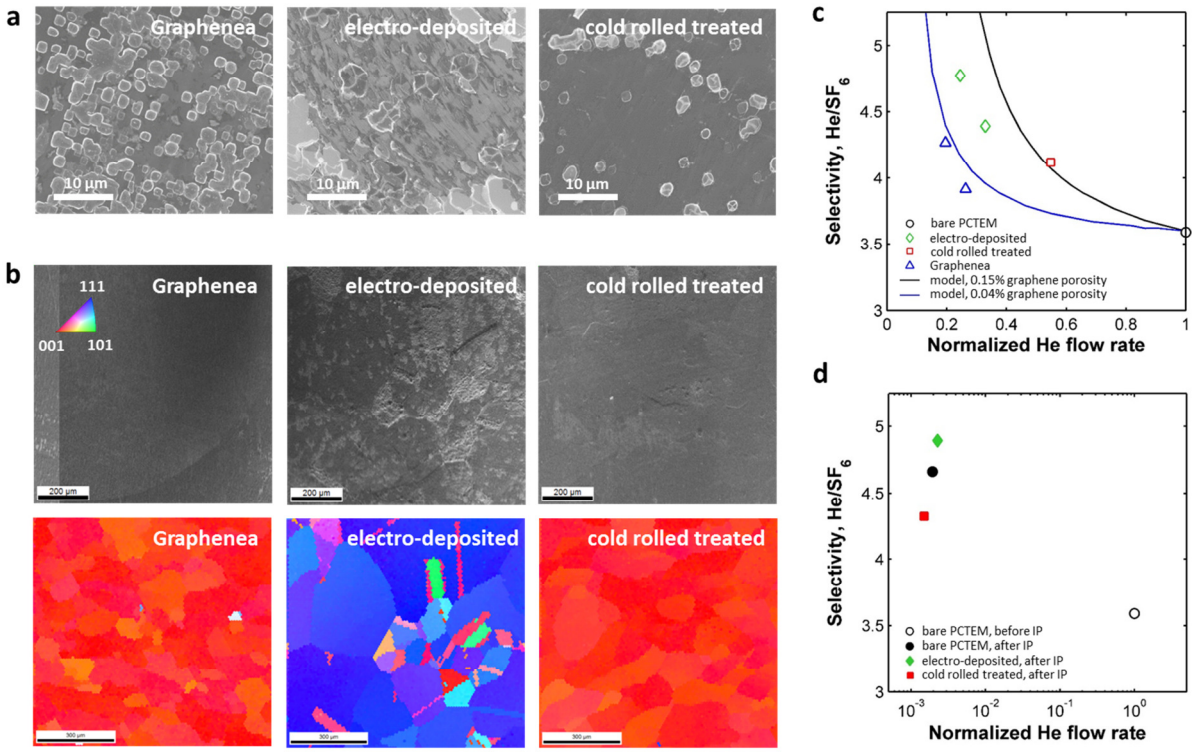

Figure 5. a) Etch tests on graphene on copper. Left to right: Commercially available graphene, CVD on electrodeposited foil, and on cold-rolled foil. b) Comparison of etch test and copper grain orientation measured by EBSD reveals the concentration of defects on grains with awkward orinetations. c) Gas flow rate measurements on different graphene samples on polycarbonate. Higher selectivity denotes predominance of smaller defects in electrodeposited foils. Higher helium flow indicates greater occurrence of large defects during handling. d) After interfacial polymerization, graphene on cold-rolled copper has the lowest leakage.

rejection. However, the flux of water and rejection of other solutes agreed with a relatively simple continuum modeling approach that accounted for the finite size of the solutes and concentration polarization in the long pores of the polycarbonate membrane on which the graphene is supported (Figure 4c).

The negative leakage of NaCl was partly due to imperfect sealing of leakages for NaCl, highlighting the need for further minimizing leaks in order to achieve more accurate measurements that reflect transport across graphene pores. Therefore, we also investigated the parameters that influence quality of graphene during synthesis by chemical vapor deposition (CVD) on copper foil. To characterize defects in graphene, we performed etch tests where the graphene-on-copper was exposed to ammonium persulfate, a copper etchant. Any defects in graphene allow the underlying copper to be etched, providing a simple and robust method to assess defects in graphene. By increasing the synthesis temperature, using copper with different grain orientations, and adding a second step in synthesis where a higher amount of methane was introduced in the furnace, we were able to synthesize graphene by CVD with a defect density that was significantly lower than that of the best commercially available graphene (Graphenea Inc.) (Figure 5a). Electron back-scattering diffraction (EBSD) revealed a very interesting insight- that defects in graphene tend to be greatly exacerbated when the copper grains are oriented at awkward angles with respect to the surface of the copper foil such that none of the primary crystal facets are aligned to the surface (Figure 5b). We then assessed the leakage through graphene using gas transport measurements. We found that the graphene that exhibited the best quality in the etch tests was also the most impermeable after sealing defects with interfacial polymerization (which is excellent at sealing large tears introduced during handling, but not at sealing smaller defects introduced during synthesis) (Figure 5c,d).

This study demonstrated the ability of controlling mass transport across a monolayer of graphene by creation of a high density of tunable sub-nanometer pores. The measurements demonstrated clearly that a single layer of graphene was capable of performing as a filtration membrane, as suggested by molecular dynamics simulations. The measured water flow rates and solute rejections were consistent with those predicted by theory. This study also established a platform that allows for measurement of the transport properties imparted by different pore creation methods in graphene and other 2D materials.

Investigating the combined effects of ion irradiation and plasma etching on pore creation and transport:

Since many of the pores created by the above-mentioned study were smaller than the size of a water molecule, a key question is whether it is possible to enlarge pores by use of stronger etch methods to allow for more flexibility in tuning of mass transport. Generating a higher density of pores that permit selective passage of water molecules will permit membranes with higher permeance, and would allow for flexibility in pore creation for a range of different applications. The ability to tune pore size will also permit better understanding of how the pore structure and density corresponds to the transport properties. Additionally, since we had observed that the leakage sealing was being compromised during the $KMnO_4$ wet etch process, an etch method that did not damage the leakage sealing polymer was desired.

We therefore investigated the effects of ion bombardment to nucleate defects, and oxygen plasma as a stronger etch, also recently reported to create pores by Surwade et al (*Nature Nanotechnology*, 2015). Specifically, a two-step process of ion bombardment at a vertical angle and $7x10^{13}$ ions cm^{-2} at 1 kV, followed by oxygen plasma was sought, substituting for the oxidation with chemical

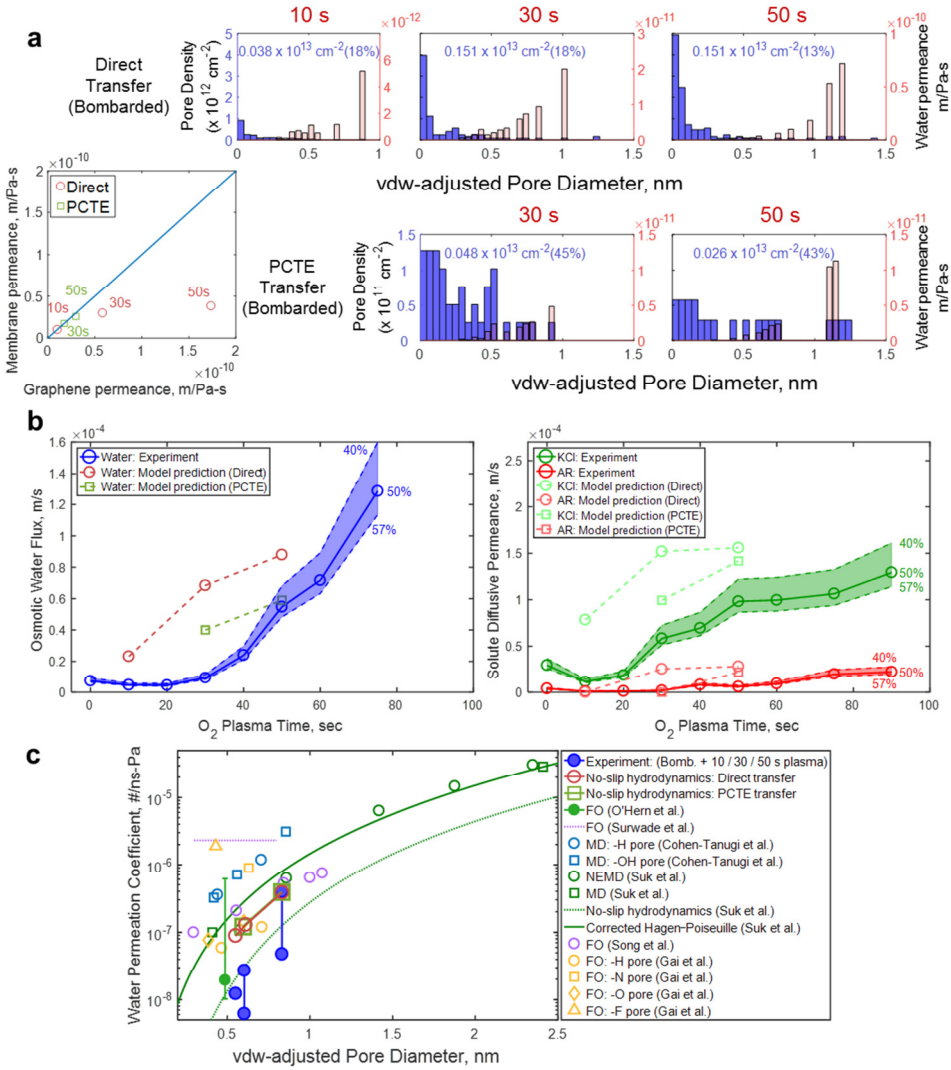

Figure 6. Analytical modeling and analysis of transport across nanoporous graphene. (a) Carbon vdw-adjusted pore diameter distribution from direct (top) and PCTE (bottom) transfer. For each bin, theoretical water permeance of graphene from no-slip hydrodynamics was estimated from all water permeable vdw-adjusted pores. Density of water permeable pores is indicated in blue, and their fraction compared to all vdw-adjusted pores is indicated in parentheses. Bottom left panel compares theoretical water permeance of graphene to that of entire membrane (graphene + PCTE) subject to concentration polarization at Π_{Draw} = 22.6 atm. (b) Comparison of experiments to analytical models with pores from direct (circle-dotted) and PCTE (square-dotted) transfer. Dotted lines enveloping the experimentally measured values represent the upper and lower bounds corresponding to different fractions (40% and 57%) of unsealed PCTE pores. Left: Osmotic water flux predicted by model using no-slip hydrodynamics and internal concentration polarization. Right: KCl and Allura Red diffusive permeance predicted by continuum diffusion theory. (c) Comparison of this work to reported molecular dynamics simulations and experiments. Water permeation coefficient and weighted pore diameter from experiment and model prediction with pores from direct and PCTE transfer are considered. For all distributions and transport data points, vertical ion bombardment was performed at density ~6 × 10^{13} cm^{-2}.

etchant. The oxygen plasma etch, being a surface etch, did not damage the leakage sealing polymer, as seen by the low rates of transport across a leak-sealed membrane after 60 s plasma etch in the absence of graphene (Fig. 6).

For the same ion bombardment conditions, we studied the permeance of the membrane to water under forward osmosis, and to diffusion of KCl and Allura Red dye. For select membranes, we

attempted additional leakage sealing by introduction of polyethylenimine (PEI) and PEG-NHS that cross-links with amine groups in PEI, and observed that the rejection improved.

Interestingly, we observed a decrease in all transport rates for 10-20 s plasma exposure. The origin of this decrease is unclear, but it could arise from closing of pore defects due to addition of functional groups, or to attraction of different kind of surface contamination due to the plasma treatment. Beyond 30 s, we observed that the water flux increased rapidly. The resultant water permeance was ~9.5 L m^{-2} bar^{-1} h^{-1} for 50-60 s plasma, which is comparable to nanofiltration membranes and more than 5 times greater than the permeance obtained after permanganate etching. By varying the oxygen plasma time, the selectivity of membranes can be tuned to exhibit size-selective transport of ions and molecules. Tuning the pore size and density with oxygen plasma may lead to development of various applications with graphene membranes including nanofiltration, dialysis, or desalting. To relate transport properties to pore size distribution, pristine and ion-irradiated graphene was subjected to oxygen plasma treatment and imaged using STEM (Fig. 6). The results clearly showed that ion irradiation enhanced plasma etching, leading to a greater pore density. However, some large pores were observed in the ion-bombarded and etched graphene that are not consistent with the measured transport properties. A large number of 5/7 ring and similar defects were also observed, which did not grow into pores. These preliminary results suggest that vertical ion bombardment at $7x10^{13}$ cm^{-2} may be too high for pore creation, leading to coalescence of pores. Inclined bombardment at moderate density provided the best selectivity. The maximum selectivity between KCl (hydrated diameter ~ 0.66 nm) and Allura Red (~ 1 nm) was ~40.

Assessing and understanding the critical role of defects in graphene membranes:

An important issue for graphene membranes is to understand the origin and role of defects, and to be able to quickly assess the severity of defects in graphene. Conventional methods for analysis of graphene such as Raman spectroscopy and conductivity do not inform regarding its ability as a barrier to mass transport, which is its most critical function in membranes.

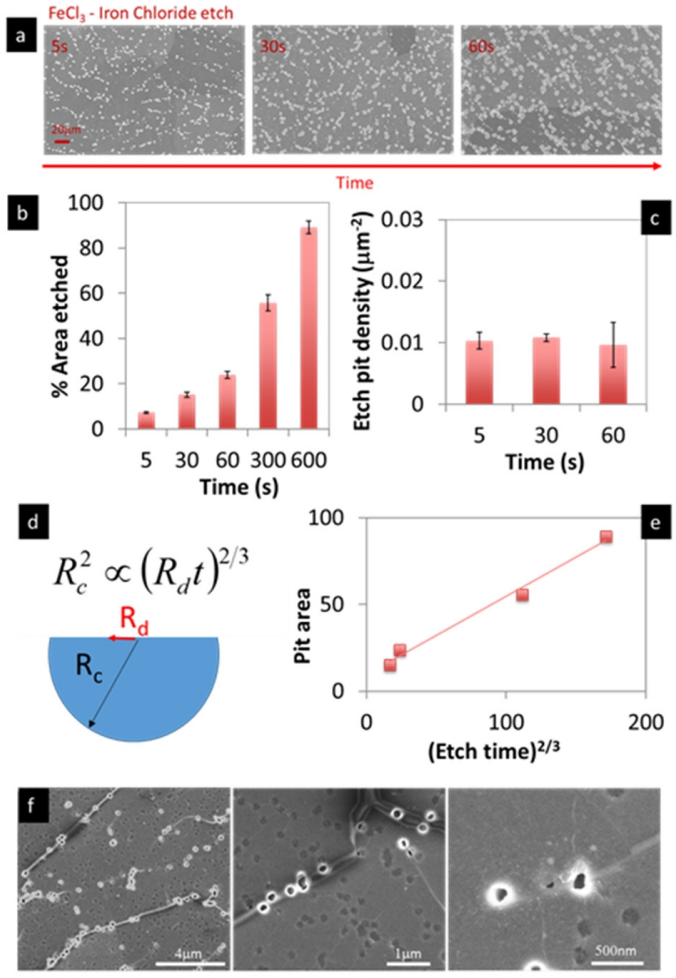

Figure 7. a) Scanning electron images of graphene on Cu foil after placing a drop of 0.1 M $FeCl_3$ for 5, 30 and 60s and rinsing in DI water. b) Percentage of etched area and c) etch pit density calculated from images in (a). d,e) Scaling model and fit to the scaling model for etch pit. f) Scanning electron images of defects on wrinkles in graphene transferred to polycarbonate track etched membranes.

Furthermore, the variability in quality and leakage between different suppliers of graphene was evident over the course of this project. The most detrimental defects are those in the few-nanometer range, which are hard to detect and hard to seal. To address this challenge, we attempted to place the copper etch test (see Fig. 5) on a firm foundation by quantitatively understanding the influence of etch time on defect density and defect area, probing the limits of detecting defects, and assessing how the etch test results corresponded to transport measurements (Fig. 7). The results indicated that the etch pits grow in a manner that is governed by mass transport across the defect, with a weak scaling with defect size to the $1/3^{rd}$ power allowing for detection of defects down to an estimated size of ~1 nm. Verification of this scaling, and the constant density of defects seen regardless of the etch time or even with electrochemical etch suggests that the etch test can easily and reliably provide a measure of the quality of graphene synthesized by CVD. Using the etch test as a guiding metric, we also developed recipes for CVD synthesis of graphene that exhibited a very low defect density, with approximately micrometer-scale spacing between defects (Fig. 5).

A key question was whether the defects observed with the etch test are consistent with the transport measurements (in the absence of pore creation or leakage sealing). The observed defect density should contribute negligibly to leakage, however, we observed that the mass transport measurements (diffusion of KCl, Allura Red, and pressure-driven fluid flow) did not agree with the density of defects predicted by the etch test. However, upon further examination, it was discovered that the source of the discrepancy is that, in the actual membrane, wrinkles give rise to additional leakage (Fig. 7f). These wrinkles are formed due to the thermal expansion mismatch between graphene and copper during cooling after CVD synthesis. They are also the weakest in terms of mechanical strength and the ability to withstand pressure.

We also examined transport across single-crystal graphene membranes made from graphene grown on SiC. The resulting membranes are free of grain boundaries, which have been speculated to give rise to leakage. In contrast to these expectations, we observed that even single-crystal graphene without any grain boundaries harbors defects, and that these defects provide for selective transport between molecules. These results suggest that focusing on single-crystal graphene may not necessarily resolve issues of defects in graphene membranes.

These results provide a simple quality control test for assessing the barrier properties of graphene, and also indicate that wrinkles are the weakest link in terms of both the barrier properties of graphene as well as its mechanical strength.

Bottom-up synthesis of nanoporous graphene by tuning the CVD process:

The observations of intrinsic nanoscale defects in graphene raise the question as to whether the defect formation process can be adequately controlled to directly synthesize graphene with nanoscale pores. This line of approach is similar to the nitrogen doping approach originally proposed, but much simpler to implement. Based on the observation that graphene quality is poorer when the CVD synthesis temperature is lower, we examined low-temperature CVD graphene for pores in its lattice and also for selective transport (Fig. 8).

Raman spectra were measured for CVD graphene samples synthesized at $\geq$1000 ^{0}C showed clear peaks corresponding to high quality graphene *i.e.*, 2D (~2700 cm^{-1}), G (~1600 cm^{-1}) and a complete absence of the D peak (~1350 cm^{-1}). However, a decrease in CVD process temperature was accompanied by a clear and distinct increase in the D peak, particularly for temperatures $\leq$ 950 ^{0}C indicating the presence of defects and dangling bonds in the graphene lattice. To assess the size-

selectivity and mass transport, we measured the diffusive flux across the graphene + PCTE and normalized it with the diffusive flux across the bare PCTE support membrane for solutes such as KCl (salt, hydrated K+ and Cl- ions ~0.66 nm), L-Tryptophan (amino acid, ~0.7-0.9 nm, 204 Da), Allura Red Dye (food coloring dye, ~1 nm, 496 Da), Vitamin B12 (vitamin, ~1-1.5 nm, 1355 Da) and Lysozyme (egg protein, ~3.8-4 nm, 14300 Da). A decrease in graphene CVD growth temperature led to selective transport in the order KCl > L-Tryptophan > Allura Red > Vitamin B12, which suggests the presence of nanometer and sub-nanometer sized pores in graphene. High resolution transmission electron microscopy images of the graphene synthesized at 900 °C confirmed the presence of nanometer sized defects in the graphene lattice, in agreement with transport measurements and Raman spectra.

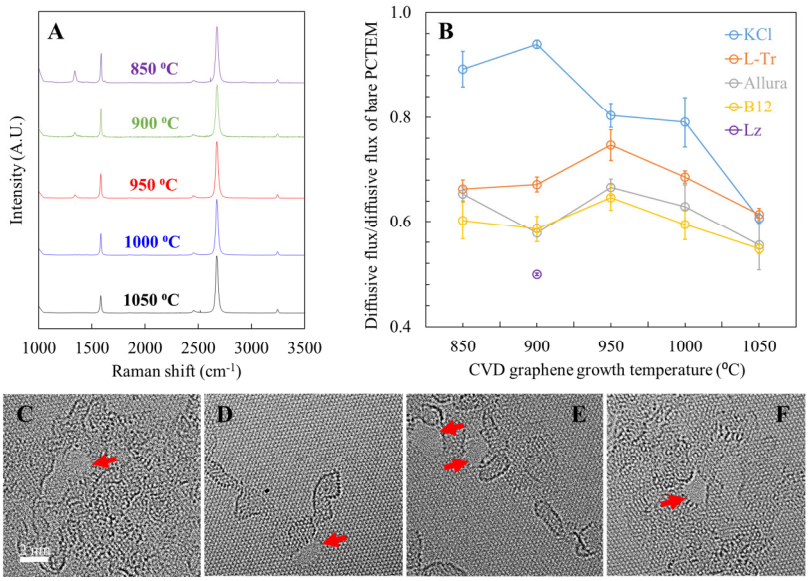

Figure 8. Assessment and characterization of nanometer scale defects in CVD graphene. A) Raman spectra for monolayer graphene synthesized at different temperatures by chemical vapor deposition (CVD). The emergence of the D peak at lower synthesis temperature is indicative of defects in the hexagonal graphene lattice. B) Diffusive transport across CVD graphene transferred on to PCTE normalized by transport across bare PCTE support indicates preferential transport of KCl ~0.66nm compared to L-Tryptophan (Tr, ~0.7-0.9nm), Allura red dye (Allura, ~1nm), Vitamin B12 (B12, ~1-1.5nm) and Lysozyme (Lz, ~3.8-4 nm). Such diffusive transport is indicative of sub-nanometer to nanometer sized defects in graphene. C-F) High resolution transmission electron microscopy images of the graphene synthesized at 900 ^{0}C shows the presence of nanometer sized defects/holes (marked by red arrows)xpected for fluctuations due to binding/unbinding events with a characteristic binding timescale.

Further, by solution-casting of porous polyether sulfone (PES) supports on the as-grown nanoporous CVD graphene, we demonstrated large-area (>5 cm^2) nanoporous graphene membranes for dialysis. The membranes showd size-selective diffusive transport and effective separation of small molecules and salts from a model protein, with ~2-100× increase in permeance along with better/comparable selectivity to state-of-the-art commercially available polymeric dialysis membranes.

Study of ion transport across isolated pores in graphene:

The above studies with macroscopic graphene membranes are essentially ensemble measurements, which mask the nature of ionic transport through individual pores in graphene. To understand the transport mechanisms and heterogeneity between different pores, we developed a chemical-resistant flow cell apparatus for measurement of currents through graphene suspended over small (~20-40 nm diameter) pores in silicon nitride membranes designed to isolate single or few pores (Figure 9a,b). This technique essentially resembles the "patch clamp" that was instrumental in elucidating the behaviors of biological ion channels.

Based on knowledge of intrinsic defects in graphene (Boutilier et al, *ACS Nano* 8, 841, 2014), the size of the silicon nitride pore was chosen to provide a high probability of isolating one or few defect pores. We observed a range of ionic conductance in 10 different experiments spanning the region between an open silicon nitride nanopore and the leakage current without a pore. Empirical fit based on molecular dynamics simulation (Suk et al *J Chem Phys* 140, 084707, 2014) placed the pore sizes in the sub-2 nm range (Figure 9c), where we expect continuum descriptions to break down. This sub-continuum pore size range may be expected to exhibit interesting behaviors including ion selectivity depending on ion hydration effects, as is exhibited by biological ion channels that have a similar range of pore sizes.

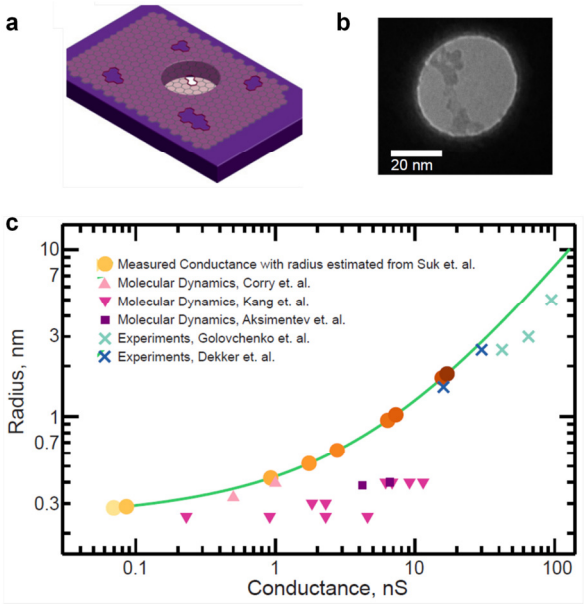

Figure 9. a) Schematic of device to isolate single or few pores in graphene. b) TEM image of isolated area of graphene. c) Conductance of measured areas (circle) with upper bound estimate of pore size from Suk et al (green line). Crosses denote previously measured graphene pores, while triangles denote MD simulation results.

These investigations revealed some remarkable ion transport behaviors in intrinsic pore defects in graphene. First, we observed heterogeneous cationic selectivities in the sub-nanometer graphene pores, as evident from the marked differences in pore conductance observed for different salts that do not scale with bulk conductivity (Figure 10a). These experiments also revealed that the pores switched conductance with time, as indicated by the large scatter in conductance values in some cases but not in others (grey circles in Figure 10a). To address this issue, we directly assessed ion selectivity by measuring the membrane potential with two salts (e.g. KCl and LiCl) on either side of the membrane. This method enabled us to directly measure a sub-nanometer pore exhibiting extremely high anion rejection, and significant cation-cation selectivity between K^+, Mg^+, and Li^+. We also observed strong current rectification while measuring transport with ruthenium salt of 1.2 nm cation size on one side and KCl on the other, consistent with size-based exclusion of ruthenium

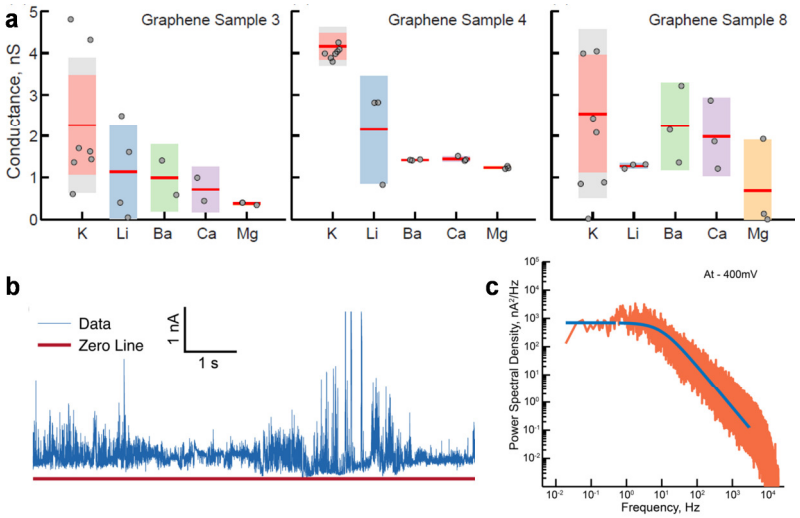

Figure 10. a) Conductance of three different graphene devices for chloride salts of different cations. Circles indicate individual measurements and shaded area indicated uncertainty. b) Fluctuations of current observed in a pore with 1 M KCl, resembling well-known current fluctuations in biological ion channels. c) PSD of the current shows a threshold that is expected for fluctuations due to binding/unbinding events with a characteristic binding timescale.

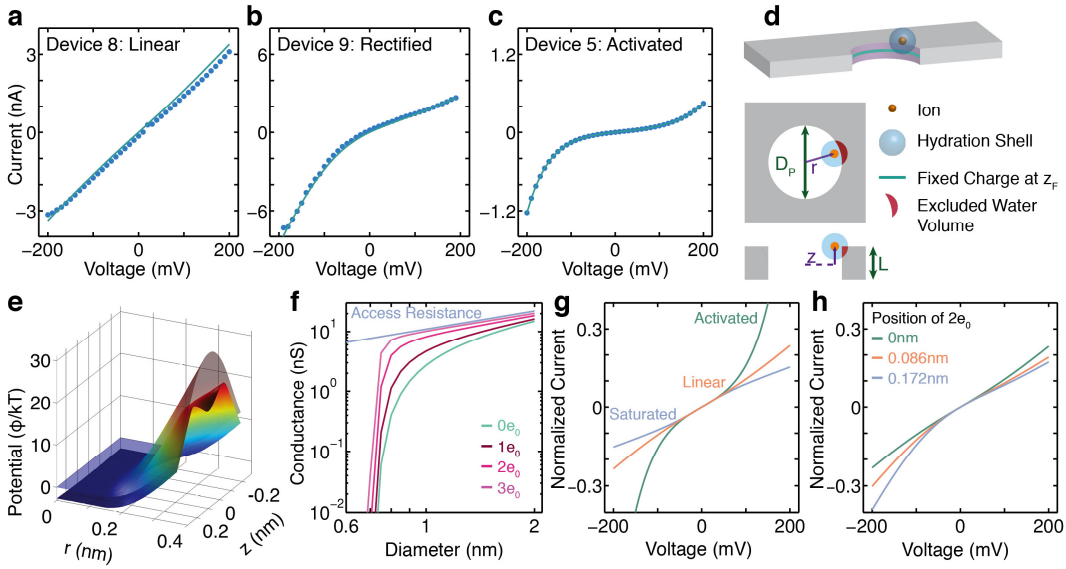

Figure 11. Current-voltage (I-V) characteristics reflect ion hydration and electrostatic effects. (a – c) Experimentally measured (●) I-V curves in 1 M KCl (linear, rectified, and activated respectively) with fits from transport model (—). (d) Model geometry for the graphene nanopore. Red areas represent the excluded volume of the hydration shell for a given ion position. (e) Free energy profile for K^+ ions in a 0.8 nm diameter nanopore without electrostatic contributions (translucent) and with electrostatic effects ($2e^-$, opaque). (f) Conductance vs. nanopore radius for different pore charge. Uncharged pore agrees with[8], and conductance transitions from hydration-limited to access resistance-limited (—) as the charge increases. (g) Pore diameter and charge determine whether I-V curves are linear (—1.0 nm, $0e^-$), activation-type nonlinear (— 0.7 nm, $0e^-$), or saturation type nonlinear (—0.85 nm, $6e^-$). (h) Current rectification as the charge moves off-center for a 0.85 nm diameter pore with $2e^-$.

salt while permitting the transport of K^+.

To understand these data, we developed a model of ion transport that accounted for steric, electrostatic, and hydration interactions of ions with the graphene pore. We found that the model could quantitatively fit the non-linear I-V curves with pore size, pore charge, and charge location being the only free parameters (Figure 11). The pore size and charge determined the conductance based on trade-offs between electrostatic and hydration interactions. The offset of charge position with respect to the plane of graphene determined whether the pores exhibit rectification or not.

Secondly, we observed voltage-dependent gating and switching behavior of graphene nanopores (Figure 10b). Voltage gating was accompanied by increase in 1/*f* noise with a threshold at a certain frequency (Figure 10c) and non-linear I-V curves. The threshold frequency is expected if the fluctuations arise from binding/unbinding events, for example ion or proton binding to a functional group at the pore (Kasianowicz & Bezrukov, *Biophys J* 69, 94, 1995). The threshold frequency corresponds to the timescale of the process: at frequencies below the characteristic frequency of switching, the fluctuations are averaged out. These short timescale fluctuations contrast with the voltage-independent long-timescale switching seen in Figure 9a, which may be due to ion-binding effects or blocking due to surface adsorbed contaminants. This is further supported by the conductance model that is able to mimic the large amplitude of the switching events for reasonable changes in the nanopore charge; addition of $2e^-$ changes current from 0.13 to 1.9 nA for a 0.8 nm pore, whereas addition of $1e^-$ changes current from 1.1 to 2.2 nA for a 1.05 nm pore, directly correlating with two of the observed switching behaviors of the pores. Remarkably, in both cases the current fluctuations occured only for negative voltage bias, which is expected for an

asymmetrically located binding site where the proton or ion concentration increases as the local electric potential is modulated by either positive or negative (but not both) voltage biases.

These studies are beginning to illustrate parallels and contrasts between the behavior of graphene nanopores and biological ion channels, and will provide insights into the ion transport mechanisms in subnanometer conduits and graphene membranes.

Study of gas transport across nanoporous graphene membranes:

Whereas the focus of this work was on understanding mass transport across graphene in the aqueous phase, we also performed measurements on transport of gas molecules. These membranes were made by placing graphene on a porous anodized alumina membrane. Pores were created in graphene by ion irradiation and plasma etching. The experiments showed that, as plasma etching increased the graphene porosity, the membranes showed an increase in selectivity followed by a decrease in selectivity as the pores presumably became enlarged and non-selective. Gas transport across the porous graphene was modeled using Monte Carlo method and accounting for the steric hindrance provided by graphene pores of a given distribution to the given gas molecule. The model

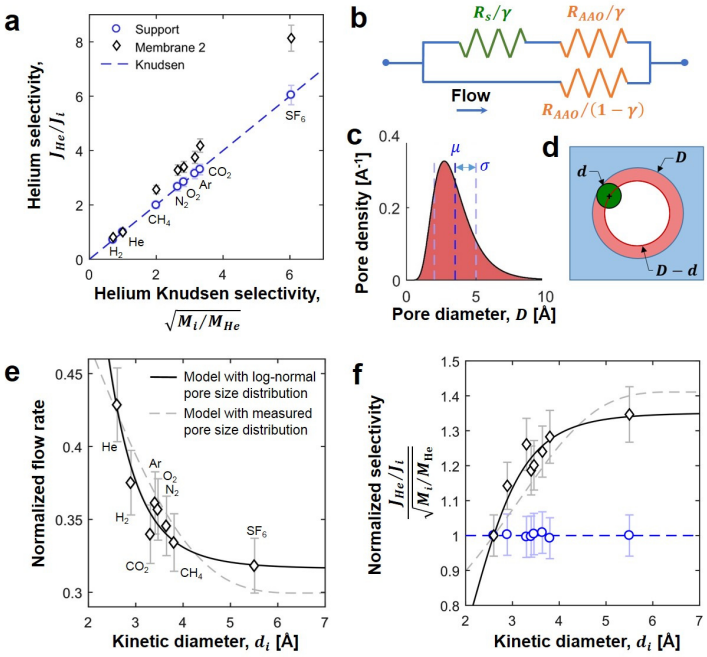

Figure 12. Ratio of helium flow rate to that of other gases, plotted against the corresponding Knudsen selectivity. **b-d,** Membrane permeance model. The equivalent resistance model (b), accounts for areas with graphene, which has a resistance due to selective pores of R_s and covers a fraction γ of the membrane, defects, where there is no graphene, and the resistance of the support pores, R_{AAO}. The model is applied using two different assumed selective pore size distributions, the measured distribution on Fig. 3a and a generic log normal distribution. The log-normal pore size distribution is (c) specified by a mean (μ) and standard deviation (σ). The effective pore size (d) available for transport through a pore of diameter D and for a gas with molecule kinetic diameter d is approximated as $D-d$. **e,** Gas flow rates, normalized by the flow rate of that gas through the AAO before graphene transfer, compared to the fitted models. **e,** Flow rate ratio of helium to other gases, normalized by the corresponding Knudsen effusion value, and compared to the models. The data plotted are for membrane 2, bombarded at 2x10^{13} ions/cm^2, after 95 s oxygen plasma exposure. The fitting parameters with a log-normal pore size distribution are $\mu = 0.0273$ Å, $\sigma = 0.0303$ Å, $\gamma = 0.684$, $\rho_s = 2.6 \times 10^{12}$ cm^{-2}, and with the measured distribution are $\gamma = 0.7000$ and $\rho_s = 2.5 \times 10^{11}$ cm^{-2}.

captured the observed trends in gas transport, and also confirmed that the mechanism of selectivity was molecular sieving. This result was the first demonstration of molecular sieving of gases across nanoporous graphene with centimeter-scale membrane area.

Products from work supported fully or in part by this project:

Peer-reviewed journal publications:

1. S. C. O'Hern, M. S. H. Boutilier, J. Idrobo, Y. Song, J. Kong, T. Laoui, M. Atieh, and R. Karnik, "Selective Ionic Transport through Tunable Subnanometer Pores in Single-Layer Graphene Membranes," *Nano Letters* **14**, 1234-1241 (2014).
2. S. C. O'Hern, D. Jang, S. Bose, J. Idrobo, Y. Song, T. Laoui, J. Kong, and R. Karnik, "Nanofiltration Across Defect-Sealed Nanoporous Monolayer Graphene," *Nano Letters* **15**, 3254-3260 (2015).
3. T. Jain, B. C. Rasera, R. Guerrero, M. S. H. Boutilier, S. C. O'Hern, J-C. Idrobo, and R. Karnik, "Heterogeneous Sub-Continuum Ionic Transport in Statistically Isolated Graphene Nanopores," *Nature Nanotechnology* **10**, 1053-1057 (2015).
4. M. S. H. Boutilier, N. G. Hadjiconstantinou, and R. Karnik, "Knudsen Effusion through Polymer-Coated Three-Layer Porous Graphene Membranes," *Nanotechnology* **28**, 184003 (2017).
5. L. Wang, C. M. Williams, M. S. H. Boutilier, P. R. Kidambi, and R. Karnik, "Single-Layer Graphene Membranes Withstand Ultrahigh Applied Pressure," *Nano Letters* **17**, 3081-3088 (2017).
6. P. R. Kidambi, M. S. H. Boutilier, L. Wang, D. Jang, J. Kim, and R. Karnik, "Selective Nanoscale Mass Transport across Atomically Thin Single Crystalline Graphene Membranes," *Advanced Materials* **29**, 1605896 (2017).
7. M. S. H. Boutilier, D. Jang, J. Idrobo, P. R. Kidambi, N. G. Hadjiconstantinou, and R. Karnik, "Molecular Sieving Across Centimeter-Scale Single-Layer Nanoporous Graphene Membranes," *ACS Nano* **11**, 5726–5736 (2017).
8. P. R. Kidambi, D. Jang, J. Idrobo, M. S. H. Boutilier, L. Wang, J. Kong, and R. Karnik, "Nanoporous Atomically Thin Graphene Membranes for Desalting and Dialysis Applications," *Advanced Materials* **29**, 1700277 (2017).
9. D. Jang, J. Idrobo, T. Laoui, and R. Karnik, "Water and Solute Transport Governed by Tunable Pore Size Distributions in Nanoporous Graphene Membranes," *ACS Nano* (accepted).

Conference presentations:

1. S. C. O'Hern, Y. Song, M. S. H. Boutilier, S. Bose, J.-C. Idrobo, T. Laoui, M. Atieh, J. Kong, and R. Karnik, "Tuning the Selectivity of Graphene Membranes by Nucleation and Growth of Pore Defects," IMECE 2013 ASME International Mechanical Engineering Congress & Exposition, Nov. 15-21, 2013, San Diego, CA, USA.
2. S. C. O'Hern, Y. Song, M. S. H. Boutilier, S. Bose, J.-C. Idrobo, T. Laoui, M. Atieh, J. Kong, and R. Karnik, "Selective Molecular Transport through Controlled Pores in Large-Area Graphene Membranes," MRS Fall Meeting, Dec. 1-6, 2013, Boston, MA, USA.
3. S. C. O'Hern, M. S. H. Boutilier, S. Bose, D. Jang, J-C Idrobo, Y. Song, T. Laoui, M. Atieh, J. Kong, and R. Karnik. "Selective Ionic Transport through Nanoporous Graphene," Flow 14 Conference, May 18-21, 2014, Enschede, The Netherlands.
4. T. Jain, B. C. Rasera, R. J.S. Guerrero, and R. Karnik, "Selectivity in Ionic Transport through Randomly Sampled Small Areas of CVD Graphene," Flow 14 Conference, May 18-21, 2014, Enschede, The Netherlands.
5. S. C. O'Hern, D. Jang, M. S. H. Boutilier, Y. Song, J. Idrobo, J. Kong, M. Atieh, T. Laoui, and R. Karnik, "Development of Defect Tolerant High-flux Graphene Membranes for Nanofiltration," Materials Research Society Fall Meeting, Nov. 30-Dec. 5, 2014, Boston, MA, USA.

6. D. Jang, S. C. O'Hern, P. Kidambi, M. S. H. Boutilier, Y. Song, J. Idrobo, J. Kong, T. Laoui, and R. Karnik, "Development of Defect Tolerant High-flux Graphene Membranes for Nanofiltration," North American Membrane Society Annual Meeting, May 30-June 30, 2015, Boston, MA, USA.
7. P. Kidambi, M. S. H. Boutilier, D. Jang, J. Kong, and R. Karnik, "Chemical Vapor Deposition of Atomically Thin Materials for Membrane and Barrier Applications," North American Membrane Society Annual Meeting, May 30-June 30, 2015, Boston, MA, USA.
8. R. Karnik, "Nanofluidic Transport across Single-Layer Graphene Membranes," 2015 Gordon Conference on Physics and Chemistry of Microfluidics, May 31 – June 5, 2015, West Dover, VT.
9. R. Karnik, "Nanofluidic Transport across Nanoporous Monolayer Graphene Membranes," American Chemical Society National Meeting and Exposition, August 16 – 20, 2016, Boston, MA.
10. D. Jang, S. C. O'Hern, P. Kidambi, M. S. H. Boutilier, Y. Song, J. Idrobo, J. Kong, T. Laoui, and R. Karnik, "Water and Molecular Transport across Nanopores in Monolayer Graphene Membranes," 68th Annual Meeting of the APS Division of Fluid Dynamics, Nov 22 - 24, 2015, Boston, MA.
11. P. Kidambi, A. Mok, D. Jang, M. Boutilier, L. Wang, J. Kong, and R. Karnik, "Chemical Vapor Deposition of Atomically Thin Materials for Membrane Applications," 68th Annual Meeting of the APS Division of Fluid Dynamics, Nov 22 - 24, 2015, Boston, MA.
12. M. Boutilier, N. G. Hadjiconstantinou, R. Karnik, "Development of Macroscopic Nanoporous Graphene Membranes for Gas Separation," 68th Annual Meeting of the APS Division of Fluid Dynamics, Nov 22 - 24, 2015, Boston, MA.
13. D. Jang, M. S. H. Boutilier, J. Idrobo, T. Laoui, and R. Karnik. "Tuning Water-Selective Pores in Monolayer Graphene Membranes for Nanofiltration," 2016 MRS Spring Meeting, Mar 28 - Apr 1, 2016, Phoenix, AZ.
14. P.R. Kidambi, D. Jang, M. Boutilier, L. Wang, S. C. O'Hern, and R. Karnik, "Tuning Porosity in Graphene and other Atomically Thin Materials for Size Selective Membrane Applications by Chemical Vapor Deposition," 2016 MRS Spring Meeting, Mar 28 - Apr 1, 2016, Phoenix, AZ.
15. M. S. H. Boutilier, D. Jang, L. Wang, P. R. Kidambi, N. G. Hadjiconstantinou, and R. Karnik, "Development of Macroscopic Nanoporous Graphene Membranes for Gas Separation," 2016 MRS Spring Meeting, Mar 28 - Apr 1, 2016, Phoenix, AZ.
16. R. Karnik, "Exploring the Potential of Nanoporous Single-Layer Graphene as a Next-Generation Membrane Material," 2016 Annual Meeting of the North American Membrane Society, May 21 – 25, 2016, Bellevue, WA, USA.
17. M. S. H. Boutilier, D. Jang, L. Wang, P. R. Kidambi, N. G. Hadjiconstantinou, and R. Karnik, "Macroscopic Nanoporous Graphene Membranes for Molecular-Sieving-Based Gas Separation," The 69th Annual Meeting of The American Physical Society – Division of Fluid Dynamics, November 20-22, 2016, Portland, OR, USA.
18. L. Wang, C. Williams, M. S. H. Boutilier, P. R. Kidambi, and R. Karnik, "Ultra-Strong CVD Graphene Membranes Capable of Withstanding High Pressure," 2016 MRS Fall Meeting, November 27 – December 2, 2016, Boston, MA, USA.
19. P.R. Kidambi, M. Boutilier, L. Wang, D. Jang, and R. Karnik, "Analysis and Origin of Defects in Graphene as an Ultrathin Barrier for Mass Transport," 2016 MRS Fall Meeting, November 27 – December 2, 2016, Boston, MA, USA.
20. D. Jang, J. Idrobo, T. Laoui, and R. Karnik, "Transport across Tunable Pore Size Distribution in Macroscopic Graphene Membranes," 11th International Congress on Membranes and Membrane Processes, July 29 – August 4, 2017, San Francisco, CA, USA.
21. L. Wang, C. M. Williams, M. S. H. Boutilier, P. R. Kidambi, and R. Karnik, "Single-Layer Graphene Membranes Withstand Ultra-High Applied Pressure," 11th International Congress on Membranes and Membrane Processes, July 29 – August 4, 2017, San Francisco, CA, USA.
22. M. S. H. Boutilier, D. Jang, J. Idrobo, P. R. Kidambi, N. G. Hadjiconstantinou, and R. Karnik, "Molecular Sieving across Centimetre-Scale Nanoporous Graphene," 11th International Congress on Membranes and Membrane Processes, July 29 – August 4, 2017, San Francisco, CA, USA.

Web articles:

http://news.mit.edu/2017/graphene-high-pressure-desalination-more-productive-0424

http://news.mit.edu/2015/repair-graphene-leaks-0508

http://news.mit.edu/2015/big-range-behaviors-tiny-graphene-pores-1005

http://news.mit.edu/2014/how-to-create-selective-holes-in-graphene-0225

Networks and Collaborations:

Funding from DOE has fostered collaboration between the PI and Juan-Carlos Idrobo at ORNL, who is an expert in high-resolution electron microscopy. It has also fostered collaboration with Prof. Nicolas Hadjiconstantinou at MIT, who is an expert in numerical methods to study nanoscale transport, with Prof. Jing Kong at MIT, who is an expert in graphene synthesis, and Prof. Tahar Laoui at KFUPM, who is an expert in porous materials. Finally, this project partly supported Dr. Piran Kidambi, who has recently joined the faculty at Vanderbilt University.

Technologies/Techniques:

Techniques were developed to measure and interpret mass transport across single-layer graphene suspended over polycarbonate membranes. Methods were developed to create pores in graphene. Third, techniques were advanced to characterize pore size distributions in graphene using scanning transmission electron microscopy. Techniques were also developed to fabricate functional membranes from graphene by sealing. This technology has garnered much interest from industry and has led to follow-on sponsored research to advance the technology toward applications.

Patent Applications:

1. R. Karnik, S. Bose, M. S. H. Boutilier, N. G. Hadjiconstantinou, T. Jain, S. C. O'Hern, T. Laoui, and M. A. Atieh, "Mitigating Leaks in Membranes," PCT/US2014/063301, November 2014.
2. P. Kidambi, A. Ibrahim, T. Laoui, J. Kong, R. Karnik, "Formation of Pores in Atomically Thin Materials," US 62/418,055 Provisional Application Filed November 2016.
3. P. Kidambi, R. Karnik, D. Jang, M. S. H. Boutilier, "Techniques for Performing Diffusion Based Filtration Using Nanoporous Membranes and Related Systems and Methods," US 62/418,064 Provisional Application filed November 2016.